

Overcoming the Phase Inhomogeneity in Chemically Functionalized Graphene: The Case of Graphene Oxides

Bing Huang,^{1,*} Hongjun Xiang,^{1,2} Qiang Xu,¹ and Su-Huai Wei^{1,†}

¹National Renewable Energy Laboratory, 1617 Cole Boulevard, Golden, Colorado 80401, USA

²Key Laboratory of Computational Physical Sciences (Ministry of Education), State Key Laboratory of Surface Physics, and Department of Physics, Fudan University, Shanghai 200433, People's Republic of China

(Received 29 August 2012; published 19 February 2013)

The inhomogeneous phase, which usually exists in graphene oxides (GOs), is a long-standing problem that has severely restricted the use of GOs in various applications. By using first-principles based cluster expansion, we find that the existence of phase separation in conventional GOs is due to the extremely strong attractive interactions of oxygen atoms at different graphene sides. Our Monte Carlo simulations show that this kind of phase separation is not avoidable under the current experimental growth temperature. In this Letter, the idea of oxidizing graphene on a single side is proposed to eliminate the strong double-side oxygen attractions, and our calculations show that well-ordered GOs could be obtained at low oxygen concentrations. These ordered GOs behave as quasi-one-dimensional narrow-gap semiconductors with quite small electron effective masses, which can be useful in high-speed electronics. Our concept could be widely applied to overcome the phase inhomogeneity in various chemically functionalized two-dimensional systems.

DOI: [10.1103/PhysRevLett.110.085501](https://doi.org/10.1103/PhysRevLett.110.085501)

PACS numbers: 61.48.Gh, 64.75.Jk, 68.43.-h

The prospects of graphene electronics have stimulated extensive studies in recent years, mostly because of the extremely high carrier mobility in graphene [1]. However, many emerging applications, e.g., transistors and photovoltaics, require a semiconducting material. Therefore, much effort has been devoted to induce an energy gap in graphene-based materials [2–9]. It has been demonstrated that an energy band gap can be achieved through either quantum confinement [3,4] or chemical functionalization [5–9]. Compared to nanopatterning of graphene, chemical functionalization of graphene is easier to scale up in production. As a precursor to chemically modified graphenes, graphene oxides (GOs), which were first discovered in an experiment by Benjamin Brodie almost 150 years ago [10], have recently been extensively revisited owing to their tunable electronic, mechanical, and optoelectronic properties depending on the degree of oxidation [6,8,9,11–13].

Unfortunately, almost all the GOs obtained in the current experiments exhibit some degree of inhomogeneity, with nonuniform band gap and low carrier mobility [6,8,9] (e.g., 2–200 cm² V⁻¹ S in thermally reduced GOs [14] compared to the typical value of 200 000 cm² V⁻¹ S in suspended graphene [1]). These poor electronic properties caused by an inhomogeneous phase make GO an unappealing candidate for high-quality electronics. As a result, although it was discovered over one century ago [10], GO itself has quite limited applications and is most often modified by chemical or thermal treatments with the goal of removing oxygen groups from GO surfaces and producing graphene [15]. In order to utilize GO in modern electronics, it is therefore important to understand several fundamental issues in this system: why does the inhomogeneous phase generally exist in GOs, and is it possible to

achieve uniform ordered GOs under some special conditions?

Although extensive experimental [6,9,15,16] and theoretical studies [11–13,17–19] have been carried out to understand the structures of GOs, these fundamental issues are still not clear. In this Letter, by employing first-principles based cluster expansion (CE) and Monte Carlo (MC) simulations, we have elucidated the physical origin of the inhomogeneous phase in GO structures as being due to the extremely strong attractive interactions of oxygen atoms at the different sides of graphene, which gives rise to the clustering of oxygen atoms (i.e., phase separation) at reduced oxygen concentrations. The calculated phase diagram shows that it is impossible to overcome the phase separation at reduced oxygen concentrations at the normal experimental temperature (usually less than 2000 K) for the synthesis of well-ordered partially oxidized GOs. To overcome this problem, the concept of oxidizing graphene on a single side is proposed to remove the strong double-side oxygen attractions, which may be achieved by oxidizing epitaxial graphene on certain inert substrates. Five well-ordered, narrow-gap single-sided GOs (SSGOs) with small electron effective masses are discovered at low oxygen concentrations, which are suitable for various applications. Generally, homogeneous SSGOs at low oxygen concentrations can be achieved at a temperature around 1250 K, which is significantly lower than the conventional (double-sided) GOs and could be realized under the current experimental conditions.

Experimental measurements have confirmed that GOs obtained from the commonly used Hummers method contains oxygen mainly in the form of epoxy (i.e., the bridge

site oxygen) as well as hydroxyl (i.e., -OH) groups [6,8,9,15]. However, the hydroxyl groups are less stable, and so, after annealing to produce the thermally reduced GOs, most of the hydroxyl groups are removed and the epoxy groups play the dominant role in GOs [20]. Moreover, recent experimental progress also shows that it is possible to produce GOs with only epoxy groups [20,21], e.g., by using atomic oxygen as dopant [21]. Therefore, in this study, we will focus on GOs with only epoxy groups. Theoretically, GOs are usually evaluated by first-principles methods only for specific structures with certain oxygen concentrations [11–13,18,19]. Apparently, a full understanding of the energy and structure relationships of GOs should consider a very large number of possible configurations, but direct exploration of this large configuration space using *ab initio* methods is not practical. Here, we study the structural diversity and stability of GOs using a first-principles based CE method commonly used for alloys [22]. For GOs with only epoxy groups, the two spin variables in the CE model are oxygen or vacancy occupying the bridge site in these pseudoalloy GOs.

The basic idea of CE is to expand the energies of a GO configuration into energy contributions of cluster figures (single atoms, pairs, triples, etc.) based on a generalized Ising Hamiltonian [22]:

$$E(\sigma) = J_0 + \sum_i J_i \hat{S}_i(\sigma) + \sum_{j<i} J_{ij} \hat{S}_i(\sigma) \hat{S}_j(\sigma) + \sum_{k<j<i} J_{ijk} \hat{S}_i(\sigma) \hat{S}_j(\sigma) \hat{S}_k(\sigma) + \dots, \quad (1)$$

The index i, j , and k run over all bridge sites, and $S_m(\sigma)$ is +1 when it is occupied by oxygen and -1 if it is not. The first two terms on the right-hand side of Eq. (1) define the linear dependence of the energy of the alloys as a function of the alloy composition x , while the third and fourth terms contain all pair and three-body interactions, respectively, etc. Every cluster figure is associated with a coefficient J_α , that gives the energy contribution of the specific cluster figure and is called the effective cluster interaction. In principal, the CE is able to represent any GO alloy energy $E(\sigma)$ by an appropriate selection of the values of J_α . The unknown J_α can be determined by fitting them to the energies of some selected configurations obtained through *ab initio* calculations, as implemented in ATAT code [23]. As the measure of CE quality, the cross-validation (CV) score obtained by a least-squares fit to *ab initio* energies is adopted.

To calculate the phase diagram of GOs, MC simulations, which sample a semi-grand-canonical ensemble, are carried out in which the energetics of the GO alloys are specified by the CE Hamiltonian. In this ensemble, the energy and concentration of an alloy with a fixed total number of active atoms (i.e., oxygen and vacancy) are allowed to fluctuate while temperature and chemical potentials are externally imposed. The simulation box contains 50×50 graphene unit cells, which is proved to be large enough to avoid the size effect. The phase boundary tracking method [24] is used to determine the equilibration and average times for

the given precision on the average concentration of the alloy. Lattice vibrational energy within the framework of harmonic approximation is also taken into account [25], which is useful to obtain improved phase diagrams.

All first-principles calculations are performed with the VASP package [26] using the projector augmented wave method in conjunction with the spin-polarized local-density approximation to the electron exchange and correlation. The kinetic energy cutoff for the plane wave basis is set to 550 eV. All GO geometries are represented by supercells with a 20 Å vacuum region in the normal direction. Γ -centered k -point mesh is carried out over the Brillouin zone for all the structures, ensuring approximately the same k -point density among different-sized supercells. All the structures are fully relaxed until the force on each atom is less than 0.01 eV/Å. The band structure calculations are carried out by hybrid functional calculations [27], which can describe the electronic structure better than local density approximation.

The traditional route to produce GO involves several steps: oxidation of graphite using the Hummers method [6,8,9,15] and then exfoliation of GO layers by chemical methods. After this kind of treatment, both sides of graphene are oxidized. The ratio of O/C has a maximum value of 1 and can be reduced by thermal reduction to desired values [6,8,9,15]. In our calculations, the formation energy (E_f) of oxygen adsorption is defined as

$$E_f = E(\text{CO}_x) - \mu_C - x\mu_O \quad (2)$$

where μ_C is set to be the energy of graphene per C atom. The relative stability between various GOs is independent of the particular choice of μ_O . Our preliminary calculations show that two oxygen atoms occupying two neighboring bridge sites are quite unstable with very high energy, agreeing with previous results [11–13,18,19]; thus these kinds of structures are excluded in our CE calculations. Here the E_f of selected 120 CO_x structures, containing at most 32 atoms in each unit cell, are calculated using *ab initio* methods with the maximum O/C ratio of 1, as shown in Fig. 1(a). In the ground state of CO_1 , epoxy pair chains are aligned along a zigzag direction and the C-C bonds under epoxy pairs are broken [17,20]. Compared with graphene (D_{6h} symmetry), the magnitude of the lattice vectors of CO_1 (D_{2h} symmetry) is increased from 2.46 to 3.02 Å and the angle between them is 129.5° versus the 120° of an ideal hexagonal lattice.

These J_α values defining the CE are obtained by fitting to the density functional theory energies of those selected GO structures, and the CE with the lowest CV score of 18 meV/atom contains 26 J_α up to four-point clusters, as shown in Fig. 1(b). Apparently, J_α are dominated by negative values (attractive interactions for oxygen atoms) and the strengths of negative J_α are significantly larger than those of positive ones (repulsive interactions for oxygen atoms). Interestingly, we find that these negative J_α are largely (~60%) contributed by the interactions of

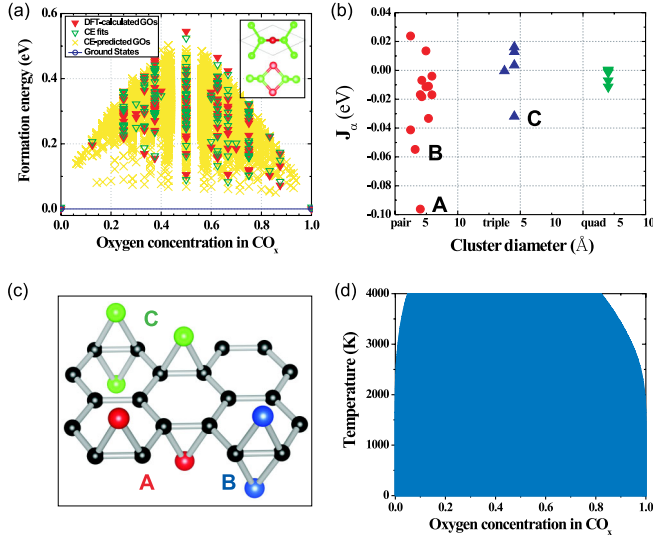


FIG. 1 (color online). (a) The calculated formation energies E_f of CO_x (with respect to graphene and CO_1) along with the corresponding CE fits as a function of oxygen concentration x in the GO system. The E_f of 25000 symmetry-inequivalent structures calculated from CE are also plotted here. Inset: the structure of CO_1 . (b) Effective cluster interactions J_α as a function of cluster diameter, fitted with CE (the empty and point clusters are excluded). (c) The cluster figures associated with the two largest negative J_α values for pairs [marked as A and B in (b)] and the largest negative J_α value for triple cluster [marked as C in (b)] are shown as different colors. (d) The MC-calculated phase diagram in CO_x alloys. The area of phase separation in this phase diagram is also shaded blue.

oxygen atoms at the different graphene sides. For example, the two largest negative J_α values for pairs [marked as A and B in Fig. 1(b)] are contributed by the interactions between the nearest and third-nearest oxygen atom pairs at different sides, while the largest negative J_α for triple cluster oxygen interaction [marked as C in Fig. 1(b)] is a combination of A and B, as shown in Fig. 1(c). Clearly, this kind of extremely strong oxygen attractions prefer to form the CO_1 pattern locally. The constructed CE are then used to calculate the E_f of all enumerated symmetry-inequivalent structures (~ 25000) up to 32 atoms/cell, and the results are shown in Fig. 1(a). Overall, we find that there are no intermediate ground states for $0 < x < 1$, which is consistent with the dominant negative values of J_α for short-range pairs and strongly indicates that the ground states of CO_x ($x < 1$) will separate into a graphene phase and a CO_1 phase. As the typical values of x in CO_x in the current experiments are usually smaller than 0.5, we can understand that inhomogeneous phase generally exists in almost all the GO samples. Our calculations explain quite well the recent experimental discovery that thermally reduced GO is separated into unoxidized graphene regions and high-oxidized GO regions that have a quasihexagonal unit cell with an unusually high 1:1 O:C ratio [20].

One may expect to enhance the solubility of GO alloys at high growth temperature, which is proved to be a very

successful idea in the growth of many conventional alloys like III nitrides [28,29] and $\text{Cu}(\text{In}, \text{Ga})\text{Se}_2$ solar materials [30]. In order to investigate this possibility, the phase diagram for graphene CO_x ($0 < x \leq 1$) is calculated by MC simulations, as shown in Fig. 1(c). We find that the miscibility temperature of GO even at quite low oxygen concentration ($x \leq 0.05$) is around 4000 K, which is rather high and close to the melting point of graphite [31]. The calculated phase diagram clearly demonstrates that it is impossible to get homogeneous GOs by the conventional Hummers methods under the typical temperature for preparing thermally reduced GOs [6,8,9,15,20,21].

Because the origin of phase separation in GOs is due to the dominated attractive oxygen interactions at different graphene sides, in order to get more uniform ordered GO structures at low oxygen concentrations one must find a way to reduce the strength of double-side oxygen attractions. Here we suggest that well-ordered uniform GOs can be achieved by restricting the growth conditions [e.g., oxidizing graphene on a single side of the graphene (i.e., forming SSGOs) rather than forming conventional double-sided GOs to minimize this kind of double-side oxygen attraction], which may be achieved by oxidizing graphene on some inert substrates (such as SiO_2). For the high-oxidized SSGOs, our calculations show that it is unlikely to find a SSGO structure with $\text{O}/\text{C} \geq 0.5$ that has a lower E_f than that of $\text{CO}_{0.5}$ shown in Fig. 2(a). In the structure of $\text{CO}_{0.5}$ (C_{2v} symmetry), epoxy chains are aligned along a zigzag direction and the C-C bonds under the epoxy group are enlarged from 1.42 to 1.50 Å but without bond breaking. Compared with the CO_1 phase, the magnitude of lattice vectors of $\text{CO}_{0.5}$ is decreased to 2.63 Å.

The E_f of 160 selected SSGO structures, containing at most 48 atoms in each unit cell, with different x , are calculated, and these selected structures can reach a good CV score of 16 meV/atom including 40 J_α up to four-point clusters. After fitting from CE, we find that the significant difference between the SSGOs and double-sided GOs is that the quantity and strengths of positive J_α are comparable to the negative ones, as shown in Fig. 2(b), which indicates that cluster repulsion plays an important role at certain oxygen-oxygen distances and could result in ordered structures (See Supplemental Material for some examples of cluster figures associated with the corresponding J_α [32]). The constructed CE are carried out to calculate the E_f of all enumerated symmetry-inequivalent configurations (~ 17000) for these structures, and the results are shown in Fig. 2(a). As we expected, five well-ordered SSGOs exist with certain stoichiometry, i.e., C_{20}O_1 , C_{18}O_2 , C_8O_1 , C_{22}O_3 , and C_{14}O_2 . The ground-state checking is carried out over the whole x range, and the CE is consistent with the density functional theory-ground-state line. Our result also offers a possible explanation for the very recent experimental observation that homogeneous GOs likely exist when oxidized epitaxial graphene grows on a SiC substrate, but the physical origin is not clear in that experiment [21].

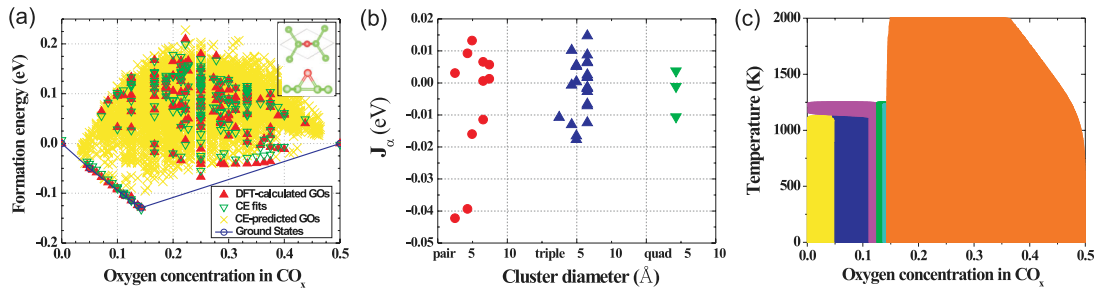


FIG. 2 (color online). (a) The calculated formation energies E_f of CO_x (with respect to graphene and $\text{CO}_{0.5}$) along with the corresponding CE fits as a function of oxygen concentration x in SSGO system. The E_f of $\sim 17\,000$ symmetry-inequivalent structures calculated from CE are also plotted here. The structure of $\text{CO}_{0.5}$ is shown in the inset. (b) Effective cluster interactions J_α as a function of cluster diameter, fitted with CE. (c) The MC-calculated phase diagram in CO_x alloys. The areas of phase separation between each two neighboring ground states in this phase diagram are also highlighted as different colors.

It is also important to understand the complete miscibility at the whole oxygen range for SSGO systems, which can provide some guidelines for the synthesis of homogeneous SSGOs in practice. The MC-simulated phase boundary between each two neighboring ground states is shown in Fig. 2(c). Differing from that of double-sided GOs, the temperature for complete miscibility in SSGOs is significantly lower, partially because the oxygen-oxygen binding becomes weaker. One interesting point is that under $0 \leq x \leq 0.11$ and $1100 \text{ K} \leq T \leq 1250 \text{ K}$, the SSGOs will separate into graphene and C_8O_1 phases (magenta area) rather than C_{20}O_1 (yellow area) or C_{18}O_2 (blue area) phases. If we consider the current experimental temperature on preparing the thermally reduced GO (less than 2000 K), the homogeneous SSGOs with $0 \leq x \leq 0.15$ and $0.36 \leq x \leq 0.50$ can be achieved, which is a significant improvement compared to that of double-sided GOs [Fig. 1(c)].

In the following, we will pay our attention to the structure and electronic properties of these discovered SSGO ground states. One common characteristic of these ground states is the epoxy chains lining up along the zigzag edge (Y axis) direction that are separated by graphene nanoribbons periodically along the armchair (X axis) direction, as shown in Fig. 3(a). The C-O bond length is 1.33 \AA and the $\angle\text{COC}$ is 143.8° in all these structures. The C-O bond type is between sp^2 and sp^3 (close to sp^2), resulting in small ripples in the Z direction. We can simply distinguish these five ground SSGO states by the widths of the separated graphene nanoribbons w (i.e., the numbers of carbon rows along the X direction), as shown in Figs. 3(a) and 3(b). For example, the structure of C_8O_1 is shown in Fig. 3(a), including one

graphene nanoribbon with $w = 8$ (see Supplemental Material for more details on the analysis of these structures [32]). These ground states presented in Fig. 3(b) have the same C_{2v} symmetry and similar band structure but with slightly different band gaps that range from 0.46 to 0.68 eV, dependent on the width of the nanoribbons. Generally, band gaps of these SSGOs are inversely proportional to the width of graphene nanoribbons, which is similar to the results obtained by Xu *et al.* [33] based on some similar but artificially constructed GO structures. Because of the similar structural characters of these ground states, it is expected that other homogenous SSGOs ($0 < x \leq 0.15$) made of these ground states (produced by high temperature) will have a similar band gap around 0.5 eV. There are some interesting electronic characteristics of these band structures, as shown in Fig. 3(c) for the example of C_{14}O_2 . Because of the quantum confinement effect induced by the epoxy chains along the X direction, the electronic properties of the C_{14}O_2 behave as one-dimensional graphene nanoribbons; i.e., the carriers transport along the Y direction. The calculated electron effective mass around the band gap is $\sim 0.06 m_e$, strongly indicating that, beyond the conventional GOs, these SSGOs may be quite useful in quasi-one-dimensional high-mobility electronics.

It is also necessary to examine whether those CE-discovered SSGO ground states are thermally stable for experimental fabrication. In order to explore this aspect, taking C_8O_1 as an example, a large supercell with 144 atoms is built and first-principles molecular dynamic simulations are performed with a Nose-Hoover thermostat at 1500 K (see Supplemental Material for the simulations on other

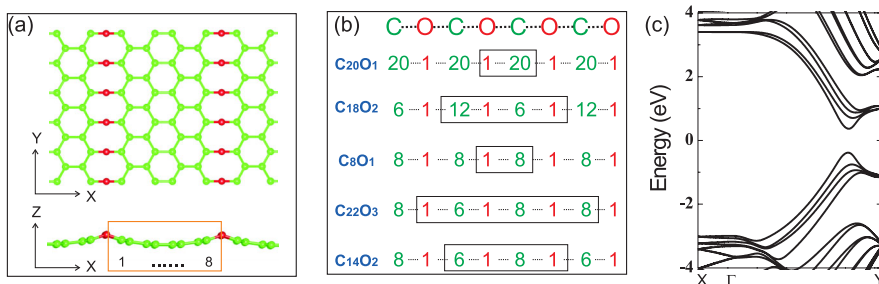


FIG. 3 (color online). (a) The optimized structure of C_8O_1 , which is one of the ground states of SSGOs. (b) Schematic drawing of the arrangement of the epoxy chain and graphene nanoribbon parts in these five ground states, i.e., C_{20}O_1 , C_{18}O_2 , C_8O_1 , C_{22}O_3 , and C_{14}O_2 . The primitive cell is enclosed by the rectangular line. (c) The calculated band structure for C_{14}O_2 . The Fermi level is set to zero.

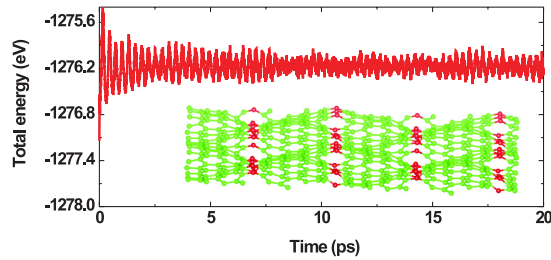


FIG. 4 (color online). The energy fluctuation of the C_8O_1 supercell as a function of the molecular dynamic simulation step at 1500 K. A snapshot of the simulated system is also shown in the inset.

ground states and the substrate effect [32]). Figure 4 shows the fluctuation of total energy as a function of simulation time. After 20 ps, we find no structural destruction of the C_8O_1 layer, except that the large thermal fluctuations induced a rippled structure (the ripple amplitude is around 2.5 Å in the Z direction), as shown in Figure 4. This strongly indicates that the sp^2 -like bonding between oxygen and carbon atoms is quite stable even under high temperature.

In summary, by employing first-principles based cluster expansion and Monte Carlo simulations, we have addressed the physical origin of the observed inhomogeneous phases in GO samples, which has hindered the potential application of GOs. To overcome this problem and achieve uniform GOs, we proposed oxidizing graphene only on a single side. Using a cluster expansion approach, several well-ordered, narrow-gap GOs with small electron effective masses are discovered at low oxygen concentrations, which are suitable for various electronic applications. Our idea could go beyond the discussed GO case and be widely applied to overcome the phase inhomogeneity in various chemically modified two-dimensional systems.

The work at NREL is supported by the U.S. Department of Energy under Contract No. DE-AC36-08GO28308. H.X. also acknowledges the support by NSFC, the Special Funds for Major State Basic Research, FANEDD, and Eastern Scholar program.

*bing.huang@nrel.gov

†Suhuai.wei@nrel.gov

- [1] A. K. Geim and K. S. Novoselov, *Nat. Mater.* **6**, 183 (2007).
- [2] T. Ohta, A. Bostwick, T. Seyller, K. Horn, and E. Rotenberg, *Science* **313**, 951 (2006).
- [3] M. Y. Han, B. Ozyilmaz, Y. Zhang, and P. Kim, *Phys. Rev. Lett.* **98**, 206805 (2007).
- [4] X. Li, X. Wang, L. Zhang, S. Lee, and H. Dai, *Science* **319**, 1229 (2008).
- [5] D. C. Elias, R. R. Nair, T. M. G. Mohiuddin, S. V. Morozov, P. Blake, M. P. Halsall, A. C. Ferrari, D. W. Boukhvalov, M. I. Katsnelson, A. K. Geim, and K. S. Novoselov, *Science* **323**, 610 (2009).
- [6] W. Gao, L. B. Alemany, L. Ci, and P. M. Ajayan, *Nat. Chem.* **1**, 403 (2009).

- [7] L. Ci, L. Song, C. Jin, D. Jariwala, D. Wu, Y. Li, A. Srivastava, Z. F. Wang, K. Storr, L. Balicas, F. Liu, and P. M. Ajayan, *Nat. Mater.* **9**, 430 (2010).
- [8] K. P. Loh, Q. Bao, G. Eda, and M. Chhowalla, *Nat. Chem.* **2**, 1015 (2010).
- [9] Y. Zhua, S. Murali, W. Cai, X. Li, J. W. Suk, J. R. Potts, and R. S. Ruoff, *Adv. Mater.* **22**, 3906 (2010).
- [10] B. C. Brodie, *Phil. Trans. R. Soc. London* **149**, 249 (1859).
- [11] D. W. Boukhvalov and M. I. Katsnelson, *J. Am. Chem. Soc.* **130**, 10697 (2008).
- [12] J. A. Yan, L. Xian, and M. Y. Chou, *Phys. Rev. Lett.* **103**, 086802 (2009).
- [13] R. J. W. E. Lahaye, H. K. Jeong, C. Y. Park, and Y. H. Lee, *Phys. Rev. B* **79**, 125435 (2009).
- [14] C. Gomez-Navarro, R. T. Weitz, A. M. Bittner, M. Scolari, A. Mews, M. Burghard, and K. Kern, *Nano Lett.* **7**, 3499 (2007).
- [15] S. Park and R. S. Ruoff, *Nat. Nanotechnol.* **4**, 217 (2009).
- [16] K. Erickson, R. Erni, Z. Lee, N. Alem, W. Gannett, and A. Zettl, *Adv. Mater.* **22**, 4467 (2010).
- [17] H. J. Xiang, S.-H. Wei, and X. G. Gong, *Phys. Rev. B* **82**, 035416 (2010).
- [18] L. Wang, Y. Y. Sun, K. Lee, D. West, Z. F. Chen, J. J. Zhao, and S. B. Zhang, *Phys. Rev. B* **82**, 161406 (2010).
- [19] A. Bagri, C. Mattevi, M. Acik, Y. J. Chabal, M. Chhowalla, and V. B. Shenoy, *Nat. Chem.* **2**, 581 (2010).
- [20] E. C. Mattson, H. Pu, S. Cui, M. A. Schofield, S. Rhim, G. Lu, M. J. Nasse, R. S. Ruoff, M. Weinert, M. Gajdardziska-Josifovska, J. Chen, and C. J. Hirschmug, *ACS Nano* **5**, 9710 (2011).
- [21] M. Z. Hossain, J. E. Johns, K. H. Bevan, H. J. Karmel, Y. T. Liang, S. Yoshimoto, K. Mukai, T. Koitaya, J. Yoshinobu, M. Kawai, A. M. Lear, L. L. Kesmodel, S. L. Tait, and M. C. Hersam, *Nat. Chem.* **4**, 305 (2012).
- [22] L. G. Ferreira, S. H. Wei, and A. Zunger, *Phys. Rev. B* **40**, 3197 (1989).
- [23] A. van de Walle, M. Asta, and G. Ceder, *CALPHAD: Comput. Coupling Phase Diagrams Thermochem.* **26**, 539 (2002).
- [24] A. van de Walle and M. Asta, *Model. Simul. Mater. Sci. Eng.* **10**, 521 (2002).
- [25] A. van de Walle and G. Ceder, *Rev. Mod. Phys.* **74**, 11 (2002).
- [26] G. Kresse and J. Furthmüller, *Comput. Mater. Sci.* **6**, 15 (1996).
- [27] J. Heyd, G. E. Scuseria, and M. Ernzerhof, *J. Chem. Phys.* **118**, 8207 (2003).
- [28] I. Ho and G. B. Stringfellow, *Appl. Phys. Lett.* **69**, 2701 (1996).
- [29] *Handbook of Luminescent Semiconductor Materials*, edited by L. Bergman and J. L. McHale (Taylor Francis Group, Boca Raton, FL, 2011).
- [30] S.-H. Wei, S. B. Zhang, and A. Zunger, *J. Appl. Phys.* **85**, 7214 (1999).
- [31] F. P. Bundy, *Physica (Amsterdam)* **156**, 169 (1989).
- [32] See Supplemental Material at <http://link.aps.org/supplemental/10.1103/PhysRevLett.110.085501> for some examples of cluster figures associated with the corresponding J_a , more details on the analysis of the structures in Fig. 3(a), and simulations on other ground states and the substrate effect.
- [33] Z. Xu and K. Xue, *Nanotechnology* **21**, 045704 (2010).